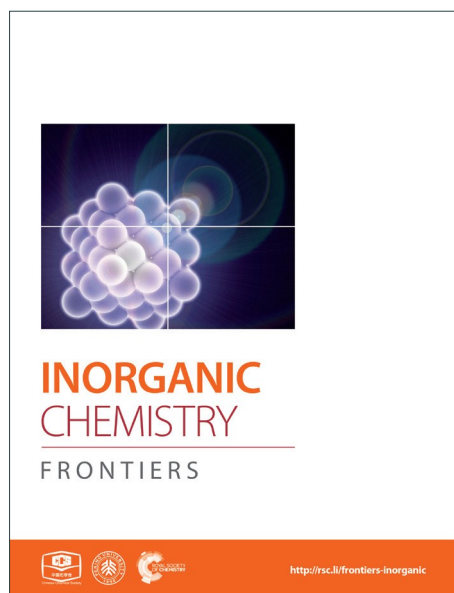
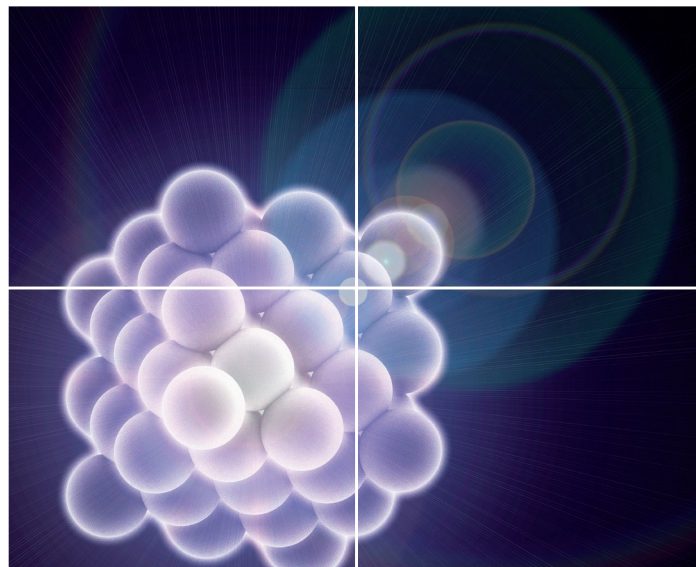


INORGANIC CHEMISTRY

FRONTIERS

Accepted Manuscript



This is an *Accepted Manuscript*, which has been through the Royal Society of Chemistry peer review process and has been accepted for publication.

Accepted Manuscripts are published online shortly after acceptance, before technical editing, formatting and proof reading. Using this free service, authors can make their results available to the community, in citable form, before we publish the edited article. We will replace this *Accepted Manuscript* with the edited and formatted *Advance Article* as soon as it is available.

You can find more information about *Accepted Manuscripts* in the [Information for Authors](#).

Please note that technical editing may introduce minor changes to the text and/or graphics, which may alter content. The journal's standard [Terms & Conditions](#) and the [Ethical guidelines](#) still apply. In no event shall the Royal Society of Chemistry be held responsible for any errors or omissions in this *Accepted Manuscript* or any consequences arising from the use of any information it contains.



Journal Name

ARTICLE

Magnetic and Photo-physical Investigations in Dysprosium and Ytterbium Complexes Involving the 4,5-ethylenedioxy-4',5'-bis(2-pyridyl-N-oxidemethylthio)tetrathiafulvalene Ligand

Received 00th January 20xx,
Accepted 00th January 20xx

DOI: 10.1039/x0xx00000x

www.rsc.org/

K. Soussi,^a J. Jung,^a F. Pointillart,^{*a} B. Le Guennic,^a B. Lefeuvre,^a S. Golhen,^a O. Cador,^a Y. Guyot,^b O. Maury,^c and L. Ouahab^a

Three lanthanide-based complexes involving a tetrathiafulvalene derivative (L) in which the lanthanide ion has a pseudo- D_{4d} symmetry have been reported. One is a dinuclear compound of formula $[Dy(hfac)_3(L)]_2$ (**1**) while the two others are isostructural and described as mononuclear complexes of formula $[Ln(tta)_3(L)] \cdot xCH_2Cl_2$ ($Ln^{III} = Dy$ and $x = 1.41$ (**2**); Yb and $x = 2$ (**3**)). The nuclearity of the species is driven by the nature of the ancillary ligands. Magnetic properties revealed that **1** and **3** behave as Single Molecule Magnets while **2** does not. The crystal field splitting of the ground multiplet state has been theoretically determined as well as the orientation of the easy axis of the ground M_J state. The results of ab initio calculations are in agreement with the experimental determinations of the anisotropy axis. Irradiation of the lowest-energy charge transfer bands of **3** lead to an intense and resolved Yb-centred emission which can be correlated to the magnetic data. Thus **3** is described as a redox-active luminescent field-induced single-molecule magnet.

Introduction

Single Molecule Magnets (SMMs) are fascinating objects which take a preponderant place in both chemists and physicist communities due to their potential applications in quantum computing,¹ high-density memory data storage devices² and spintronics.³ One of the actual challenges is to combine in the same molecule the SMM property to one or more subsequent physical properties in order to obtain a multifunctional SMM, as for instance chiral SMM,⁴ ferroelectric SMM⁵ or luminescent SMM⁶.

In this way, the use of lanthanide ions seems to be very promising since they display specific and unique physical and photophysical properties. On one side, they possess strong magnetic anisotropy and high magnetic moment making them ideal candidates for SMM⁷ and on the other side they display sharp emission lines ranging from the visible to the near infrared (NIR) region arising from f-f transitions⁸. In order to exploit this potential lanthanide ions must be coordinated to organic ligands acting as sensitizing antenna in a pre-organized way resulting in the induction of a crystal (ligand)-field that

monitor both magnetic and luminescence properties.

For several decades, tetrathiafulvalene (TTF)-based ligands were used for their electron donating ability and so for their electronic conductivity.⁹ Furthermore, their ability to form S...S short contacts and π - π stacking makes them attractive candidates as structural agent to organize the tridimensional arrangement in crystals and control the magnetic properties (magnetic isolation, SMM behaviour). In addition their strong electronic delocalization is responsible for their interesting optical properties and this push pull chromophore has been demonstrated to efficiently sensitize the lanthanide luminescence by antenna effect.¹⁰

Considerable efforts are devoted to better understand and ultimately predict the magnetic behaviour of lanthanide-based complexes and hence the crystal field effects. To that end systematic experimental works explore the magnetic properties of original structure with the aim of establishing efficient magneto-structural correlations.^{10g,11}

In parallel theoretical investigations, based on electrostatic models or high level ab initio calculations, are undertaken to estimate the lanthanide crystal field and the orientation of the magnetic axis in the molecular objects.¹²

Recently, some of us published dinuclear complexes of lanthanide involving the 4,5-bis(2-pyridyl-N-oxidemethylthio)-4',5'-ethylenedithiotetrathiafulvalene (L^1) or -methyledithiotetrathiafulvalene (L^2) ligands which displayed either SMM or luminescence behaviour but not both simultaneously.^{10g} It was demonstrated that a minor chemical change on the nature of the TTF-based ligand induced drastic magnetic modifications since $[Dy(hfac)_3(L^2)]_2$ behaves as a SMM while $[Dy(hfac)_3(L^1)]_2$ does not. In the present article, we

^aInstitut des Sciences Chimiques de Rennes UMR 6226 CNRS-UR1, Université de Rennes 1, 35042 Rennes Cedex, France.

E-mail: fabrice.pointillart@univ-rennes1.fr

^bUniversité Claude Bernard Lyon 1, Institut Lumière Matière, UMR 5306 CNRS-Université Lyon 1, 10 rue Ada Byron, 69622 Villeurbanne Cedex, France.

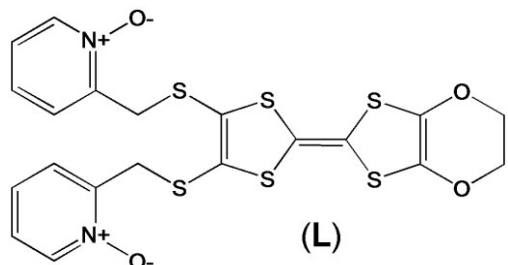
^cLaboratoire de Chimie de l'ENS-LYON-UMR 5182, 46 Allée d'Italie, 69364 Lyon Cedex 07.

† Footnotes relating to the title and/or authors should appear here.

Electronic Supplementary Information (ESI) available: [details of any supplementary information available should be included here]. See

DOI: 10.1039/x0xx00000x

continue the step-by-step study of this ligand family and report the slightly modified 4,5-ethylenedioxy-4',5'-bis(2-pyridyl-*N*-oxidemethylthio)tetrathiafulvalene (**L**) (Scheme 1) ligand featuring 4,5-ethylenedioxy moiety instead of 4,5-ethylenedithio and 4,5-dimethylthio moieties respectively for **L**¹ and **L**². This minor modification allows to optimize the magnetic properties and to combine both luminescence and SMM behaviour in a single complex.



Scheme 1. Molecular structure of **L**

Experimental section

General Procedures and Materials.

The precursors Dy(hfac)₃·2H₂O¹³ (hfac=1,1,1,5,5,5-hexafluoroacetylacetonate anion), Ln(tta)₃·2H₂O¹⁴ (Ln=Dy^{III} and Yb^{III}; tta=2-thenoyltrifluoroacetate anion) and 4,5-ethylenedioxy-4',5'-bis(cyanoethylthio)tetrathiafulvalene¹⁵ were synthesized following previously reported methods. All other reagents were purchased from Aldrich Co., Ltd. and used without further purification.

Synthesis of the ligand 4,5-ethylenedioxy-4',5'-bis(2-pyridyl-*N*-oxidemethylthio)tetrathiafulvalene (**L**).

In a three-necked flask under Argon atmosphere, 0.432 g (1 mmol) of 4,5-ethylenedioxy-4',5'-bis(cyanoethylthio)tetrathiafulvalene^{15c} was dissolved in 30 mL distilled MeOH. In the dropping funnel, 0.115 g (5 mmol) of metallic sodium was added to 10 mL distilled MeOH and added drop wise to the solution of 4,5-ethylenedioxy-4',5'-bis(cyanoethylthio)tetrathiafulvalene under stirring. After the addition was over, the solution was stirred at room temperature for 4 hours. Then, in the dropping funnel, 0.419 g (3.3 mmol) of 2-(chloromethyl)pyridine-1-oxide¹⁶ was dissolved in 20 mL distilled MeOH and added drop wise to the solution and left stirring overnight. Then 30 mL distilled water was added and stirred for 30 min, followed by the addition of 250 mL CH₂Cl₂. The resulting solution was washed with saturated NaHCO₃ and distilled water. The organic phase was dried with MgSO₄ and the solvent was removed under vacuum. The resulting powder was purified on Al₂O₃ column with 99/1 ratio of CH₂Cl₂/MeOH as eluant. Yield 200 mg (37 %). ¹H NMR (CDCl₃): δ 4.12 (s, 4H), 4.26 (s, 4H), 7.23 (m, 4H), 7.33 (m, 2H), 8.26 (m, 2H). Single crystals were obtained by slow diffusion of *n*-hexane in a concentrated CH₂Cl₂ solution of **L**.

Synthesis of complexes 1-3.

[Dy(hfac)₃(**L**)]₂ (**1**). 30.8 mg of Dy(hfac)₃·2H₂O (0.037 mmol) were dissolved in 10 mL of CH₂Cl₂ and then added to a solution of 10 mL of CH₂Cl₂ containing 20.0 mg of **L** (0.037 mmol). After

15 minutes of stirring, 25 mL of *n*-hexane were layered at room temperature in the dark. Slow diffusion leads to red single crystals which are suitable for X-ray studies. Yield 77 mg (79 %). Anal. Calcd (%) for C₇₀H₃₈Dy₂F₃₆N₄O₂₀S₁₂: C 31.73, H 1.44, N 2.12; found: C 31.99, H 1.46, N 2.11.

[Ln(tta)₃(**L**)]·xCH₂Cl₂ (Ln^{III} = Dy and x = 1.41 (**2**); Yb and x = 2 (**3**)). 0.037 mmol of Ln(tta)₃·2H₂O (32.4 mg for Dy(tta)₃·2H₂O and 32.8 mg for Yb(tta)₃·2H₂O) were dissolved in 10 mL of CH₂Cl₂ and then added to a solution of 10 mL of CH₂Cl₂ containing 20.0 mg of **L** (0.037 mmol). After 15 minutes of stirring, 25 mL of *n*-hexane were layered at room temperature in the dark. Slow diffusion leads to red single crystals which are suitable for X-ray studies. Yield 34 mg (61 %) and 39 mg (68 %) respectively for **2** and **3**. Anal. Calcd (%) for C_{45.41}H_{30.54}Cl_{2.82}DyF₉N₂O₁₀S₉: C 36.67, H 2.05, N 1.88; found: C 37.09, H 2.16, N 1.91. Calcd (%) for C₄₆H₃₂Cl₄YbF₉N₂O₁₀S₉: C 35.68, H 2.07, N 1.81; found: C 35.79, H 2.16, N 1.94.

Crystallography. Single crystals of **L** and **1** were mounted on a Nonius four circle diffractometer equipped with CCD camera and a graphite monochromated MoK_α radiation source (λ = 0.71073 Å, T = 293(2) K) while **2** and **3** were mounted on a APEXII Bruker-AXS diffractometer (MoK_α radiation source, λ = 0.71073 Å, T = 150(2) K) for data collection, from the Centre de Diffraction (CDIFX), Université de Rennes 1, France. Structures were solved with a direct method using the SIR-97 program and refined with a full matrix least-squares method on F² using the SHELXL-97 program¹⁷ for all the compounds. Crystallographic data are summarized in Table 1. Complete crystal structure results as a CIF file including bond lengths, angles, and atomic coordinates are deposited as Supporting Information.

Physical Measurements.

The elementary analyses of the compounds were performed at the Centre Régional de Mesures Physiques de l'Ouest, Rennes. ¹H NMR was recorded on a Bruker Ascend 400 spectrometer. Chemical shifts are reported in parts per million referenced to TMS for ¹H NMR. Cyclic voltametry was carried out in CH₂Cl₂ solution, containing 0.1 M N(C₄H₉)₄PF₆ as supporting electrolyte. Voltamograms were recorded at 100 mV·s⁻¹ at a platinum disk electrode. The potentials were measured versus a saturated calomel electrode (SCE) (E_{Fc/Fc+} = 0.45 V). Absorption spectra were recorded on a Varian Cary 5000 UV-Visible-NIR spectrometer equipped with an integration sphere. The luminescence spectra were measured using a Horiba-Jobin Yvon Fluorolog-3[®] spectrofluorimeter, equipped with a three slit double grating excitation and emission monochromator with dispersions of 2.1 nm/mm (1200 grooves/mm). The steady-state luminescence was excited by unpolarized light from a 450 W xenon CW lamp and detected at an angle of 90° for diluted solution measurements or at 22.5° for solid state measurement (front face detection) by a red-sensitive Hamamatsu R928 photomultiplier tube. Spectra were reference corrected for both the excitation source light intensity variation (lamp and grating) and the emission spectral response (detector and grating). Near infra-red spectra were recorded at an angle of 45° using a liquid nitrogen cooled, solid

indium/gallium/arsenic detector (850-1600 nm). The dc magnetic susceptibility measurements were performed on solid polycrystalline sample with a Quantum Design MPMS-XL SQUID magnetometer between 2 and 300 K in an applied magnetic field of 2 kOe in the 2-20 K temperature range and 10 kOe between 20 and 300 K for **3**. For **1** and **2**, 0.2 kOe is applied between 2 and 20 K, 2 kOe between 20 and 80 K and 10 kOe above 80 K. These measurements were all corrected for the diamagnetic contribution as calculated with Pascal's constants.

Computational Details.

DFT geometry optimizations and TD-DFT excitation energy calculations of the ligand **L** were carried out with the Gaussian 09 (revision A.02) package¹⁸ employing the PBE0 hybrid functional¹⁹. All atoms were described with the SVP basis sets.²⁰ The first 50 mono-electronic excitations were calculated. In all steps, a modeling of bulk solvent effects (solvent = dichloromethane) was included through the Polarizable Continuum Model (PCM),²¹ using a linear-response non-equilibrium approach for the TD-DFT step²². Molecular orbitals were sketched using the Gabedit graphical interface.²³

Wavefunction-based calculations were carried out on model structures of the Ln^{III}-based complexes **1-3** (see below) by using the SA-CASSCF/RASSI-SO approach, as implemented in the MOLCAS quantum chemistry package (versions 8.0).²⁴ In this approach, the relativistic effects are treated in two steps on the basis of the Douglas-Kroll Hamiltonian. First, the scalar terms were included in the basis-set generation and were used to determine the spin-free wavefunctions and energies in the complete active space self-consistent field (CASSCF) method.²⁵ Next, spin-orbit coupling was added within the restricted-active-space-state-interaction (RASSI-SO) method, which uses the spin-free wavefunctions as basis states.²⁶ The resulting wavefunctions and energies are used to compute the magnetic properties and g-tensors of the lowest states from the energy spectrum by using the pseudo-spin $S = 1/2$ formalism in the SINGLE-ANISO routine.²⁷ Cholesky decomposition of the bielectronic integrals was employed to save disk space and speed-up the calculations.²⁷ The atomic positions were extracted from the X-ray crystal structures. For the three complexes, only the modified TTF ligand **L** was simplified by suppressing the organic moieties beyond the central C=C bond. Moreover, in the case of the dimer **1**, only one half of the molecule was considered. For **1** and **2**, the active space of the self consistent field (CASSCF) method consisted of the nine 4f electrons of the Dy^{III} ion spanning the seven 4f orbitals, i.e. CAS(9,7)SCF. State-averaged CASSCF calculations were performed for all of the sextets (21 roots), all of the quadruplets (224 roots), and 300 out of the 490 doublets (due to software limitations) of the Dy^{III} ion. Twenty-one sextets, 128 quadruplets, and 107 doublets were mixed through spin-orbit coupling in RASSI-SO. All atoms were described by ANO-RCC basis sets.²⁸ The following contractions were used: [8s7p4d3f2g1h] for Dy, [4s3p2d] for the O directly coordinated to Dy, [3s2p] for other O atoms; [3s2p1d] for the N atoms; [4s3p] for the S atoms, [3s2p] for the C and F atoms and [2s]

for the H atoms. A similar procedure was then applied to the Yb^{III} complex **3**. The active space consisted of 13 4f electrons in seven 4f orbitals, i.e. CAS(13,7)SCF. State-averaged CASSCF calculations were performed for the seven doublets of the Yb^{III} ion, all of which were included in the RASSI-SO calculation. The effects of dynamical correlation were treated by means of a CASPT2 treatment on top of the spin-free wavefunctions. Similar basis set contractions were used except for Yb, which was described at the [8s7p4d3f2g] level.

Results and discussion

Synthesis and crystal structures

The ligand **L** (Scheme 1) was synthesized in order to study the influence of the ethylenedioxy (EDO) functionalization on the structural and then magnetic properties. First, **L** was submitted to a coordination with the Dy(hfac)₃·2H₂O precursor and the resulting dinuclear complex of formula [Dy(hfac)₃(L)]₂ (**1**) was compared to the two previously published similar compounds. **Error! Bookmark not defined.** Then the hfac⁻ ancillary ligands were substituted with the tta⁻ ones leading surprisingly to the formation of new mononuclear complexes of formula [Ln(tta)₃(L)]·xCH₂Cl₂ (Ln^{III} = Dy and x = 1.41 (**2**); Yb and x = 2 (**3**)) and not to analogues of **1**.

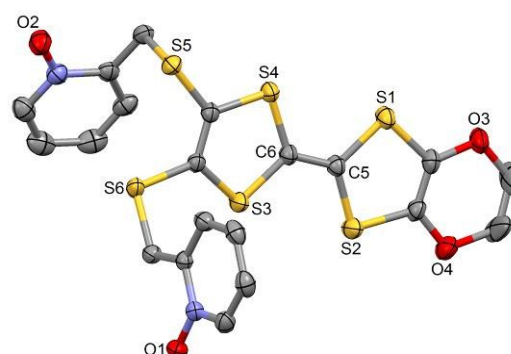


Fig. 1 ORTEP view of the ligand **L**. Thermal ellipsoids are drawn at 30% probability. Hydrogen atoms are omitted for clarity.

L crystallized in the P₂₁/a monoclinic space (Table 1). The asymmetric unit is composed of one molecule of **L** and one water molecule (Fig. 1). The central C5-C6 bond length (1.378(4) Å) confirms the neutral form of the ligand. Each 2-pyridine-*N*-oxide-methylthio arm is oriented in opposite sides with respect to the plane formed by the TTF core. The two *N*-oxide groups realize two hydrogen bonds (O1-O1w = 2.766(6) Å and O2-O1w = 2.783(6) Å) with the water molecule (Fig. 2). The **L** donors are stacked along the *b* axis with short S3...S1 contact (3.577(2) Å).

Table 1. X-ray crystallographic data for the ligand **L** and the complexes **1-3**.

Compounds	(L)	[Dy(hfac) ₃ (L)] ₂ (1)
Formula	C ₂₀ H ₁₆ N ₂ O ₅ S ₆	C ₇₀ H ₅₈ Dy ₂ F ₃₆ N ₄ O ₂₀ S ₁₂
M / g.mol ⁻¹	556.7	2705.8
Crystal system	Monoclinic	Triclinic
Space group	P2 ₁ /a (N°14)	P-1 (N°2)
Cell parameters	a = 13.2244(3) Å b = 12.1843(4) Å c = 15.3079(4) Å β = 107.908(2) °	a = 12.4879(3) Å b = 13.3816(4) Å c = 15.6598(6) Å α = 100.987(2) ° β = 90.592(2) ° γ = 107.459(2) °
Volume / Å ³	2347.06(11)	2444.19(13)
Cell formula units	4	2
T / K	293 (2)	293(2)
Diffraction reflection	5.92 ≤ 2θ ≤ 54.20	2.66 ≤ 2θ ≤ 54.18
ρ _{calc.} g.cm ⁻³	1.575	1.799
μ, mm ⁻¹	0.619	1.912
Number of reflections	27589	18277
Independent reflections	5151	10729
Fo ² > 2σ(Fo) ²	3539	7750
Number of variables	298	689
R _{int} , R ₁ , wR ₂	0.0625, 0.0509, 0.1327	0.0316, 0.0481, 0.1229
Compounds	[Dy(tta) ₃ (L)]·1.41CH ₂ Cl ₂ (2)	[Yb(tta) ₃ (L)]·2CH ₂ Cl ₂ (3)
Formula	C _{45.41} H _{50.54} Cl _{2.82} DyF ₉ N ₂ O ₁₆ S ₉	C ₄₆ H ₅₂ Cl ₄ YbF ₉ N ₂ O ₁₆ S ₉
M / g.mol ⁻¹	1486.2	1547.1
Crystal system	Triclinic	Triclinic
Space group	P-1 (N°2)	P-1 (N°2)
Cell parameters	a = 10.4634(8) Å b = 12.1092(10) Å c = 23.9781(18) Å α = 77.004(2) ° β = 86.822(2) ° γ = 74.808(2) °	a = 10.4473(3) Å b = 12.0946(4) Å c = 23.9969(7) Å α = 76.5010(10) ° β = 86.0280(10) ° γ = 74.7470(10) °
Volume / Å ³	2856.8(4)	2844.4(15)
Cell formula units	2	2
T / K	150 (2)	150 (2)
Diffraction reflection	1.74 ≤ 2θ ≤ 55.08	1.74 ≤ 2θ ≤ 55.00
ρ _{calc.} g.cm ⁻³	1.728	1.806
μ, mm ⁻¹	1.853	2.246
Number of reflections	29912	39778
Independent reflections	12500	12653
Fo ² > 2σ(Fo) ²	7773	11826
Number of variables	711	732
R _{int} , R ₁ , ωR ₂	0.0798, 0.0882, 0.2008	0.0219, 0.0387, 0.1033

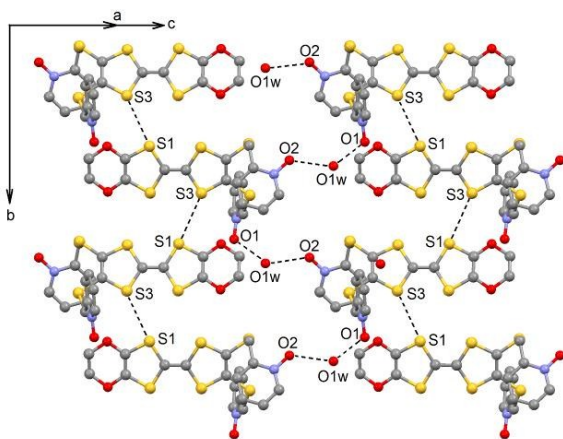


Fig. 2 Crystal packing of L highlighting the intermolecular interactions.

[Dy(hfac)₃(L)]₂ (1) crystallizes in the P-1 (N°2) triclinic space group (Table 1) and the asymmetric unit is composed of one half of the dinuclear unit (Fig. 3).

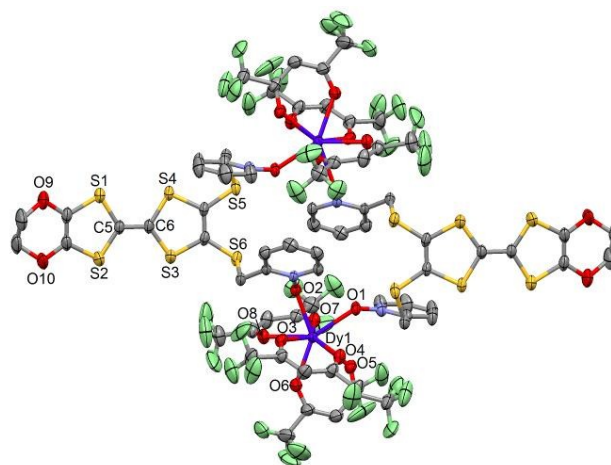


Fig. 3 ORTEP view of the dinuclear complex [Dy(hfac)₃(L)]₂ (1). Thermal ellipsoids are drawn at 30% probability. Hydrogen atoms are omitted for clarity.

Table 2. Selected bond lengths for complexes 1-3.

Compounds	1	2	3
Ln1-O1	2.345(3)	2.334(7)	2.295(3)
Ln1-O2	2.309(4)	2.349(7)	2.308(3)
Ln1-O3	2.380(4)	2.406(7)	2.361(3)
Ln1-O4	2.402(4)	2.376(7)	2.326(3)
Ln1-O5	2.370(4)	2.339(7)	2.299(3)
Ln1-O6	2.323(4)	2.327(7)	2.286(3)
Ln1-O7	2.335(4)	2.375(7)	2.332(3)
Ln1-O8	2.404(4)	2.362(7)	2.316(3)

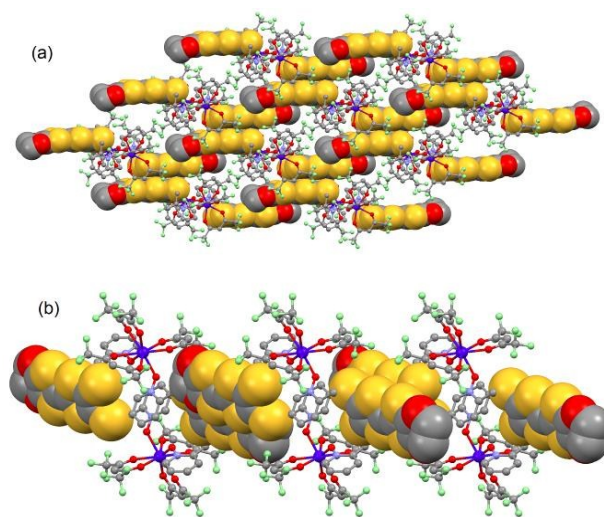


Fig. 4 Crystal packing of 1 highlighting the intermolecular interaction between L ligands and the formation of the dimers of L.

The value of the mean Dy-O_{hfac} distances is 2.359(4) Å (Table 2) that is comparable to what is observed in the previous reported dinuclear complexes involving the L¹ and L² ligands (2.340 Å).^{10g} The arrangement of the ligands leads to a

distorted square antiprism (D_{4d} symmetry) coordination polyhedron around the Dy^{III} ion. This distortion is visualized by continuous shape measures performed with SHAPE 2.1 (Table 3).³⁰ The **L** donors form dimers through S3...S5 short contact (3.691(3) Å) (Fig. 4). The shortest intra- and intermolecular Dy-Dy distances have been found equal to 9.314(5) Å and 9.039(5) Å, respectively.

[Ln(tta)₃(L)]₂ (Ln = Dy^{III} (**2**) and Yb^{III} (**3**)). Both compounds are isostructural and the description is done for **2** while the values for **3** are given between brackets. The nature of the β -diketonate of the metal precursor has been change from $hfac^-$ for **1** to tta^- for **2** and **3**. In several examples, this modification leads to change in the crystal packing but the molecule remains very similar.^{31,32} In the present case, the molecule obtained from $Ln(tta)_3 \cdot 2H_2O$ is totally different than the one obtained from $Dy(hfac)_3 \cdot 2H_2O$. **2** and **3** crystallize in the P-1 (N^2) triclinic space group (Table 1) and the asymmetric unit is composed of one mononuclear unit (Fig. 5 and S1) and two dichloromethane molecules of crystallization.

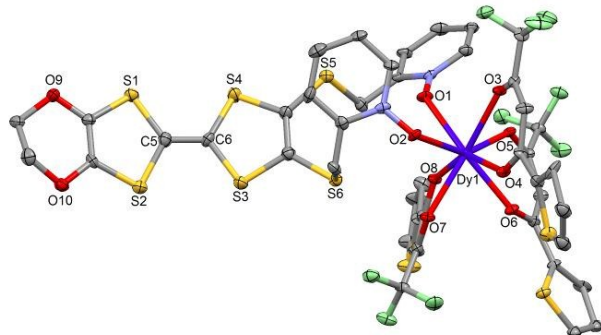


Fig. 5 ORTEP view of the mononuclear complex $[Dy(tta)_3(L)]$ (**2**). Thermal ellipsoids are drawn at 30% probability. Hydrogen atoms and dichloromethane molecules are omitted for clarity.

Table 3. SHAPE analysis of the coordination polyhedron around the lanthanide ions in complexes **1-3**.

	CShM _{SAPR-8} (square antiprism) D_{4d}	CShM _{BTTPR-8} (biaugmented trigonal prism) C_{2v}	CShM _{TDD-8} (triangular dodecahedron) D_{2d}
1	0.484	1.564	1.373
2	0.410	2.418	2.134
3	0.363	2.362	2.124

Using the $Ln(tta)_3 \cdot 2H_2O$ metal precursor, the two pyridine-*N*-oxide arms of one ligand are coordinated to the same lanthanide ion. The value of the mean Dy-O_{tta} [Yb-O_{tta}] distances is 2.359(7) [2.315(3)] Å (Table 2). The arrangement of the ligands leads to a distorted square antiprism (D_{4d} symmetry) coordination polyhedron around the Ln^{III} ion. This distortion is visualized by continuous shape measures performed with SHAPE 2.1 (Table 3).³⁰ The **L** donors are “head-to-tail” stacked to form regular pseudo one-dimensional network of **L**. Two kinds of S...S contacts are identified between i) the TTF cores (S4...S4 = 4.256(3) [4.223(4) Å] and ii) the thiophene ring and TTF core (S2...S9 = 4.067(3) [4.141(4) Å]) to form a mono-dimensional organic network along the *a*

axis (Fig. 6). The shortest intermolecular Ln-Ln distances have been found equal to 9.789(7) [9.747(5)] Å.

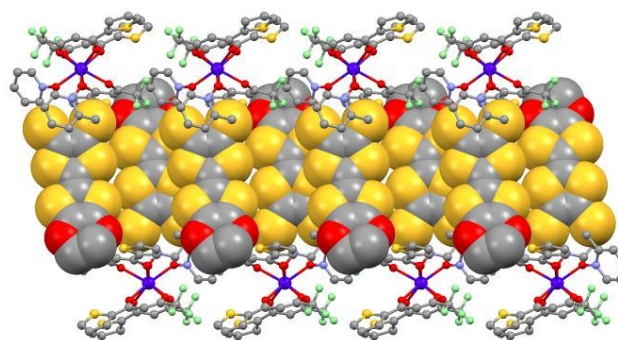


Fig. 6 Crystal packing of **2** highlighting the formation of the mono-dimensional network of **L**.

Electrochemical Properties.

The cyclic voltametry of **L** and the related complexes **1-3** are investigated to determine their redox properties. The values of the oxidation potentials are listed in Table 4. The cyclic voltammograms show two mono-electronic oxidations which correspond to the formation of a TTF radical cation and a dication, respectively (Fig. S2). Upon coordination of the electron attracting $Ln(hfac)_3$ or $Ln(tta)_3$ moieties, both $E^1_{1/2}$ and $E^2_{1/2}$ are respectively slightly cathodically and anodically shifted compare with the potentials of the free ligands. The electrochemical properties attest the redox-activity of both **L** and complexes.

Table 4. Oxidation potentials (V vs SCE, nBu_4NPF_6 , 0.1 M in CH_2Cl_2 at $100\text{ mV}\cdot\text{s}^{-1}$) of the ligand **L** and complexes **1-3**.

	$E^1_{1/2}$ / V		$E^2_{1/2}$ / V	
	$^{ox}E^1_{1/2}$	$^{red}E^1_{1/2}$	$^{ox}E^2_{1/2}$	$^{red}E^2_{1/2}$
L	0.57	0.36	0.93	0.76
1	0.52	0.40	0.96	0.81
2	0.51	0.36	0.99	0.83
3	0.50	0.33	0.96	0.77

Magnetic properties

The static and dynamic magnetic properties of the three compounds have been measured. The $\chi_M T$ vs. *T* plots are represented on Fig. 7 while the magnetization curves at 2 K are represented on Fig. S3 (it must be mentioned that the data for **1** have been divided by two to fit with one Dy^{III} per chemical unit). At room temperature the $\chi_M T$ are close to the expected values for isolated $Dy(III)$ ($^6H_{15/2}$: $14.17\text{ cm}^3\text{ K mol}^{-1}$) and $Yb(III)$ ($^2F_{7/2}$: $2.57\text{ cm}^3\text{ K mol}^{-1}$). All the $\chi_M T$ values decrease on cooling according to the thermal variation of the crystal field levels population. Nevertheless, the two $Dy(III)$ derivatives do not behave exactly the same although the coordination polyhedra look similar. The decrease is less steep for **2** than for **1** with however lower low temperature limits for **2** than for **1** ($11.2\text{ cm}^3\text{ K mol}^{-1}$ for **1** and $10.34\text{ cm}^3\text{ K mol}^{-1}$ for **2**). Differences are also visible on the magnetization curve at 2 K (Fig. S3): while magnetization of **1** saturates at a value ($4.97\text{ N}\beta$) close to that

expected for the Ising component ($M_J = \pm 15/2$) of the $^6H_{15/2}$ multiplet ground state, magnetization of **2** linearly increases with the magnetic field with higher values.

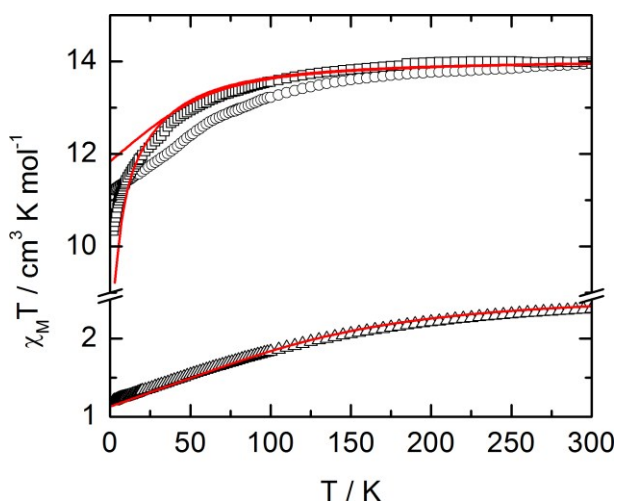


Fig. 7 $\chi_M T$ vs. T plots for compounds **1** (circles) (divided by two to fit with one Dy^{III} per chemical unit), **2** (squares) and **3** (triangles) with simulated curves from *ab-initio* calculations.

At this stage we decided to take advantage of the space group P-1 with one metallic site in general position for both **1** and **2** to perform rotating single crystal magnetometry (SI, Fig. S4-S7) and to compare the orientations of principal magnetic axes with respect to molecular geometry. The principal values of g -tensors, in the frame of the effective spin $1/2$ model, are given in Table 5 while the orientations of the principal axis with largest g value are given on Fig. 8. The most striking difference between **1** and **2** is the axiality: **1** is more Ising than **2** which suggests that **1** should be a better SMM than **2**. Furthermore the orientation of the most magnetized axis differs significantly: it is oriented toward one oxygen atom of a pyridine-*N*-oxide moiety which is also coinciding with one of $hfac^-$ ligand in **1** whereas in **2**, it is oriented between the two oxygen atoms of the two pyridine-*N*-oxide moieties. *Ab-initio* calculations (see computational details) confirm the large propensity of **1** to behave as a SMM. Indeed, at the SA-CASSCF/RASSI-SO level, both complexes present a predominant $M_J = \pm 15/2$ ground state. But due to the larger energy difference between the ground state and the first excited states in **1** than in **2** (80 cm^{-1} vs. 15 cm^{-1}), less mixing is observed for **1** than for **2** (Table S1). This behaviour is also visible in the calculated principal values of the Zeeman tensors with $g_x = 0.04$, $g_y = 0.06$, $g_z = 19.46$ for **1** whereas $g_x = 0.77$, $g_y = 3.59$, $g_z = 15.63$ for **2** (Table 5). Finally, the orientation of the main magnetic anisotropy axes are well reproduced in both Dy^{III} complexes.

For compound **3**, $\chi_M T$ varies from $1.2\text{ cm}^3\text{ K}^{-1}$ at 2 K to $2.38\text{ cm}^3\text{ K mol}^{-1}$ at room temperature. At 300 K, $\chi_M T$ is close to the expected value for the ground state multiplet $^2F_{7/2}$ ($2.57\text{ cm}^3\text{ K mol}^{-1}$). The orientation of the most magnetic axis determined from single crystal rotating magnetometry (SI, Fig. S8) is represented on Fig. 8. As for **1** and **2**, *ab initio* calculations were performed on the Yb^{III} compound **3**. However, as usual

for Yb^{III} complexes,^{11h,33} dynamical correlation effects had to be taken into account by means of CASPT2 calculations (see Computational Details). $\chi_M T$ vs. T experimental curve is well reproduced by the calculations (Fig. 7) as well as the orientation of the easy magnetic axes (Fig. 8). The ground state is well separated from the first excited state (234 cm^{-1}) and is mainly composed of $M_J = \pm 5/2$ (0.50) but with non-negligible contributions from $M_J = \pm 7/2$ (0.34) and $M_J = \pm 5/2$ (0.10). As it could have been anticipated from dc magnetic data the dynamic susceptibility of **1** and **2** differ significantly. **2** does not show any out-of-phase component of the ac susceptibility (χ_M'') whatever the temperature (down to 1.8 K) and whatever the frequency of the oscillating field (between 1 and 1000 Hz) at zero external dc field. On contrary, χ_M'' is not null in zero external field for **1** at low temperature. It shows a frequency dependent signal below 7 K in the range 1-1000 Hz (Fig. 9).

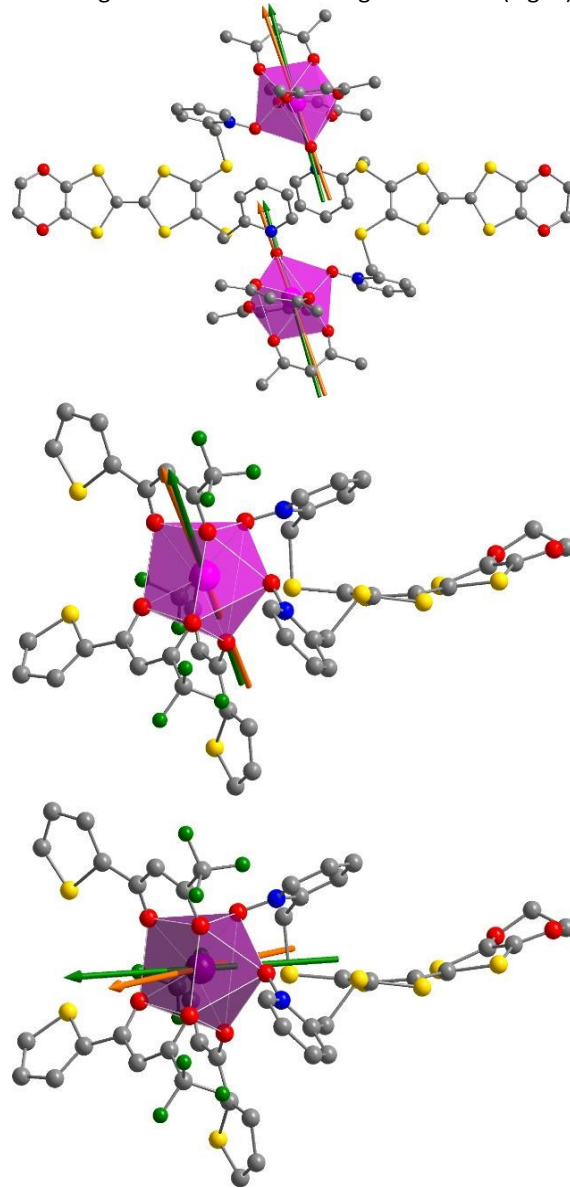


Fig. 8 Representations of the di- and mono-nuclear complexes **1** (top) and **2** (middle) with experimental (orange) and theoretical (green) orientation of the easy magnetic axes at 2 K. Orientation of the magnetic axes for compound **3** are given at the bottom.

The frequency dependences of the two components at various temperatures have been treated with an extended Debye model (see SI and Table S2) which allows plotting the thermal variations of the relaxation time τ . It follows an Arrhenius law at high temperature modulated by a thermally independent regime at low temperature (Fig. 10). The complete set of data can be adjusted with the following equation ($\tau^{-1} = \tau_0^{-1} \exp(-\Delta/T) + \tau_{TI}^{-1}$) with τ the relaxation time, τ_0 the intrinsic relaxation time, Δ the energy barrier and finally τ_{TI} the thermally independent relaxation time. The best agreement is obtained with $\tau_0 = 9 \pm 2 \times 10^{-6}$ s, $\Delta = 16 \pm 0.8$ K and $\tau_{TI} = 1.85 \pm 0.02 \times 10^{-4}$ s.

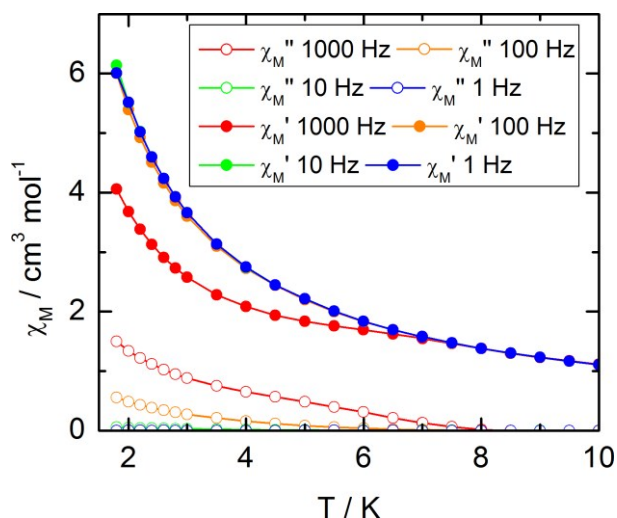


Fig. 9 Temperature variations of the ac susceptibility components, χ_M' and χ_M'' , of compound **1** measured in zero external dc field at various frequencies. Values are given for one metallic site.

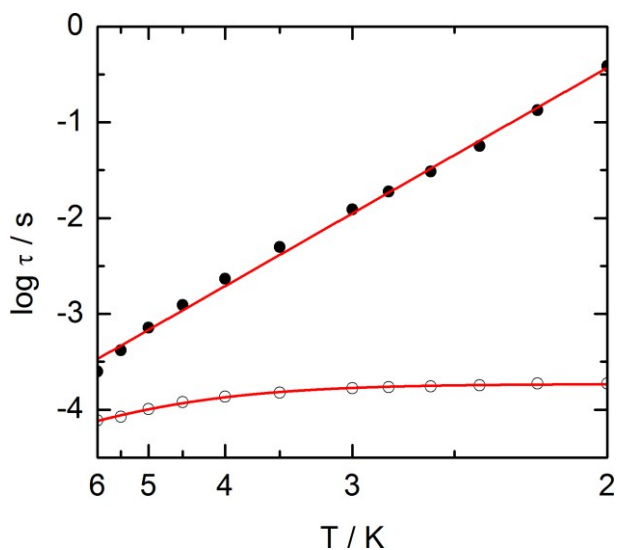


Fig. 10 Temperature variations of the relaxation time of the magnetization measured at zero external field (empty circles) and at 1 kOe (full circles) for compound **1**. Full red lines are the best fitted curves (see text).

The application of an external dc field dramatically slows the relaxation process in the thermally independent regime (Fig. S9). The application of a moderate and constant external field removes the degeneracy of the Kramer's doublet with no more direct relaxation between these two states. The most efficient

field which is the one for which the relaxation is slowest is found close to 1 kOe. Then the frequency dependences of χ_M' and χ_M'' at various temperature but recorded at 1 kOe have been treated the extended Debye model. The relaxation time obeys now to a Arrhenius law ($\tau^{-1} = \tau_0^{-1} \exp(-\Delta/T)$) with $\tau_0 = 1 \pm 0.12 \times 10^{-5}$ s, $\Delta = 21 \pm 0.3$ K. These values are of the same order of magnitude than in zero external field.

Table 5. Experimental and calculated g -tensors principal values in the frame of the effective spin $\frac{1}{2}$ model for compounds **1-3**.

	1		2		3	
	Exp.	Calc.	Exp.	Calc.	Exp.	Calc.
g_x	1.187	0.04	7.24	0.77	5.84	5.96
g_y	18.47	0.06	5.04	3.59	2.00	0.73
g_z	3.134	19.46	15.86	15.63	1.77	0.33

The normalized Cole-Cole plots (χ_M''/χ_T vs. χ_M'/χ_T) at selected temperatures between 1.8 and 7.0 K is depicted in Figure 11. They are flattened semicircles and the α values (Table S3) indicates that a single relaxation time is mainly involved in the present relaxation process.

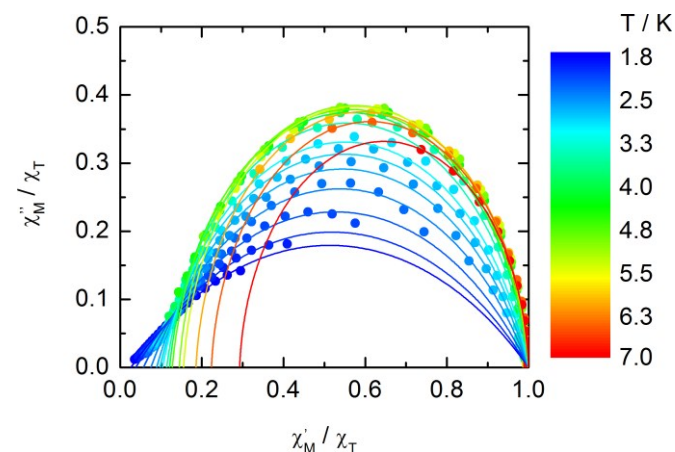


Fig. 11 Normalized Cole-Cole plots for **1** at 1 kOe between 1.8 and 7.0 K.

Compound **3** does not show any out-of-phase signal in zero external dc field whatever the temperature and the available oscillating field frequency in agreement with the calculated ground state (mainly $M_J = \pm 5/2$). However, at 1 kOe a frequency dependent out-of-phase signal shows up at lower temperatures than 4 K (Fig. 12) that may be due to the presence of non negligible contribution $M_J = \pm 7/2$ in the ground state wavefunction.

The extended Debye model (Table S4) allows to extract the temperature dependence of the relaxation which can then be treated in the frame of a thermally activated process only ($\tau^{-1} = \tau_0^{-1} \exp(-\Delta/T)$) with $\tau_0 = 1.9 \pm 0.2 \times 10^{-5}$ s and $\Delta = 6 \pm 0.3$ K (Fig. 13).

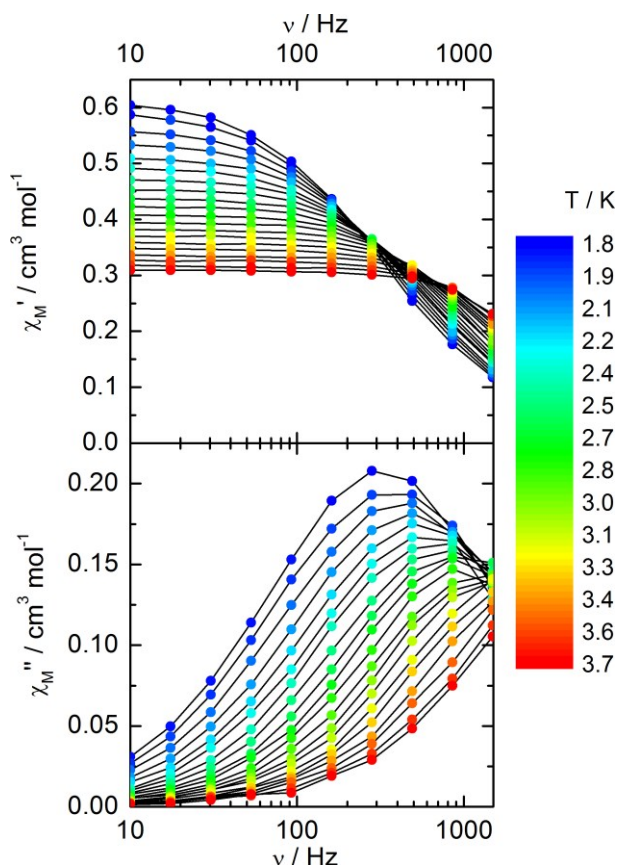


Fig. 12 Frequency variations of the ac susceptibility components, χ_M' and χ_M'' , of compound **3** measured at 1 kOe at various temperatures.

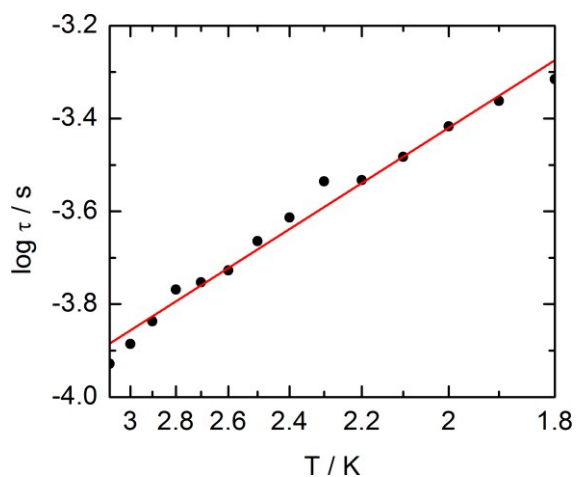


Fig. 13 Temperature variations of the relaxation time of the magnetization measured at 1 kOe for compound **3**. Full red lines is the best fitted curve (see text).

The normalized Cole-Cole plots (χ_M''/χ_T vs. χ_M'/χ_T) at selected temperatures between 1.8 and 3.0 K are flattened semicircles due to α values close to 0.05 (Fig. 14 and Table S4). This value indicates that a single relaxation time is mainly involved in the present relaxation process independently of the temperature. They almost all collapse into one semicircle which intercepts the x axis near the origin. The fast relaxing part of the magnetization is very small and is not related to the distribution of the relaxation time.

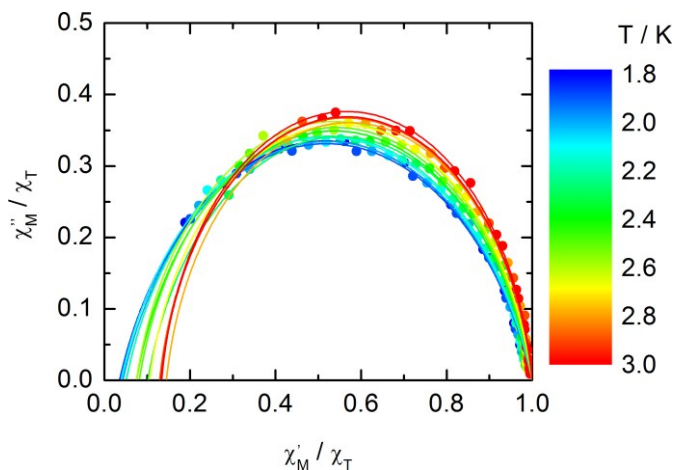


Fig. 14 Normalized Cole-Cole plots for **3** at 1 kOe between 1.8 and 3.0 K.

Photo-physical properties.

Absorption properties. The UV-visible absorption properties of **L** have been studied in a CH_2Cl_2 solution (Fig. 15a). Rationalization by TD-DFT calculations was performed following a computational strategy already used successfully on TTF-based systems.³⁴ The molecular orbital diagram and UV-visible absorption spectra were determined for **L** (Fig. 16 and 15b, Table 6). The experimental absorption curve of **L** has been decomposed into five bands (Fig. 15a and Table 6). The calculated UV-visible absorption spectrum for **L** well reproduces the experimental curve (Fig. 15a and 15b). The lowest energy band (red Gaussian decomposition) was attributed to π - π^* HOMO \rightarrow LUMO TTF to Methyl-2-Py-*N*-oxide charge transfers (ILCT) (Table 6). The absorption bands centred at 29400 cm^{-1} and 36100 cm^{-1} were also attributed to ILCT transitions while the intermediate absorption band was attributed to intra-TTF excitations. Finally the highest energy absorption band centred at 41000 cm^{-1} (purple decomposition) was attributed to Intra-Ligand IL transitions. The replacement of the ethylenedithio fragment with an ethylenedioxy one does not induce significant changes in the absorption properties. The UV-visible absorption properties of the coordination complex **3** have been first studied in solid-state (Fig. S10) and then in CH_2Cl_2 solution (Fig. 15c). The absorption spectra have been decomposed into six and seven bands respectively for the solution and solid-state measurements (Table 7). The lowest-energy additional absorption band (15500 cm^{-1}) which is observed in the solid-state spectra is due to the intermolecular CT.^{10c} Additional intense absorption excitation have been observed around 27000 - 30000 cm^{-1} that corresponds to π - π^* intra-tta⁻ excitations.^{11c} Complexations induce a weak red shift of the ligand-centered ILCT transition due to the moderate Lewis acid behavior of the $\text{Ln}(\text{tta})_3$ moieties enforcing the electron withdrawing character of the 2-pyridine-*N*-oxide fragments even if the electronic communication through the methylthio arms is expected very weak. Thus, the absorption bands are red-shifted to 1300 cm^{-1} in coordination complexes compared to those in **L**. Since the shift value is determined from the data in CH_2Cl_2 solution, this

is a first indication of the stability of the mononuclear complexes in such solvent.

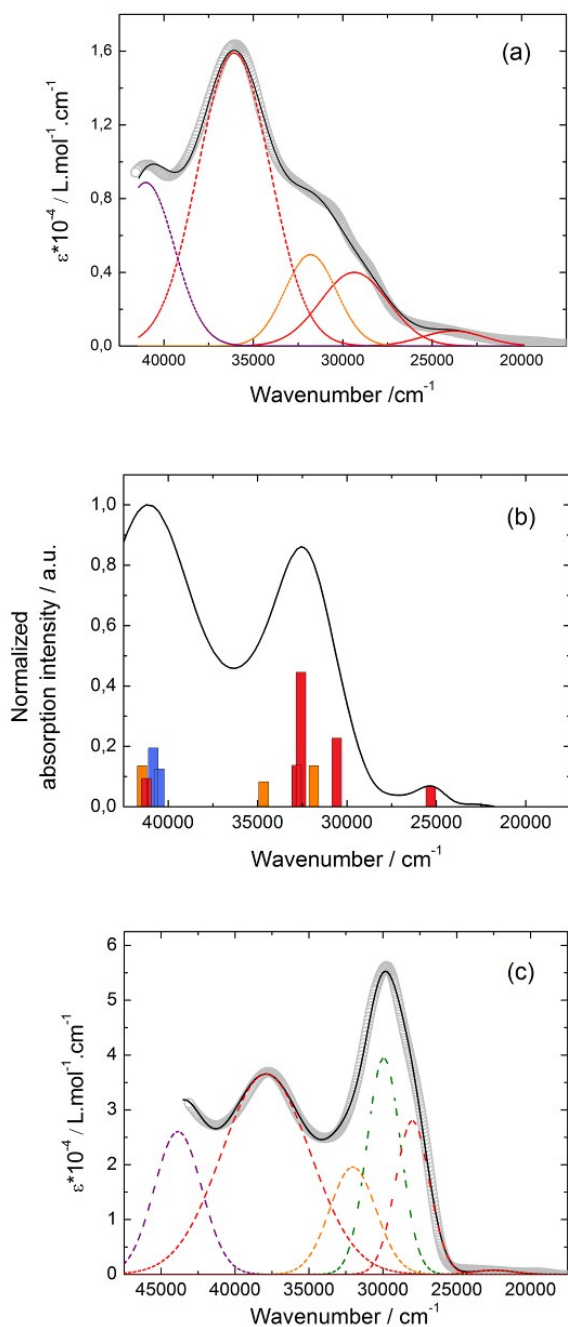


Fig. 15 (a) Experimental UV-visible absorption spectra of **L** in CH_2Cl_2 solution ($C = 4 \cdot 10^{-5} \text{ mol.L}^{-1}$) (open gray circles). Respective Gaussian decompositions (dashed lines) and best fit (full black line) ($R = 0.9988$). (b) Theoretical absorption spectra of compounds **L** (black line). The sticks represent the mean contributions of the absorption spectra for **L**. (c) Experimental UV-visible absorption spectra in CH_2Cl_2 solution of **3** ($C = 4 \cdot 10^{-5} \text{ mol.L}^{-1}$) (open gray circles). Respective Gaussian decompositions (dashed lines) and best fit (full black line) ($R = 0.9992$).

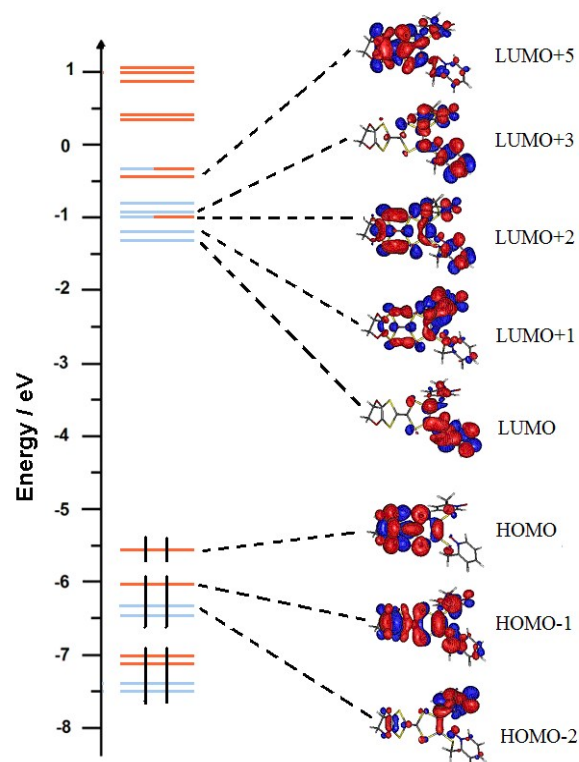


Fig. 16 Molecular orbital diagram of **L**. The energy levels of the centred TTF and 2-methylpyridine-N-oxide orbitals are represented in orange and blue, respectively.

Table 6. TD-DFT calculated absorption energies and main compositions of the low-lying electronic transitions for **L**. In addition, the charge transfer and the pure intramolecular transitions are reported. ID, IA and H, L represent the intramolecular TTF (Donor) or intramolecular 2-pyridyl-N-oxidemethylthio (acceptor), and the HOMO, the LUMO, respectively. Therefore, ILCT for Intra-Ligand Charge Transfer. The theoretical values are evaluated at the PCM(CH_2Cl_2)-PBE0/SVP level of approximation.

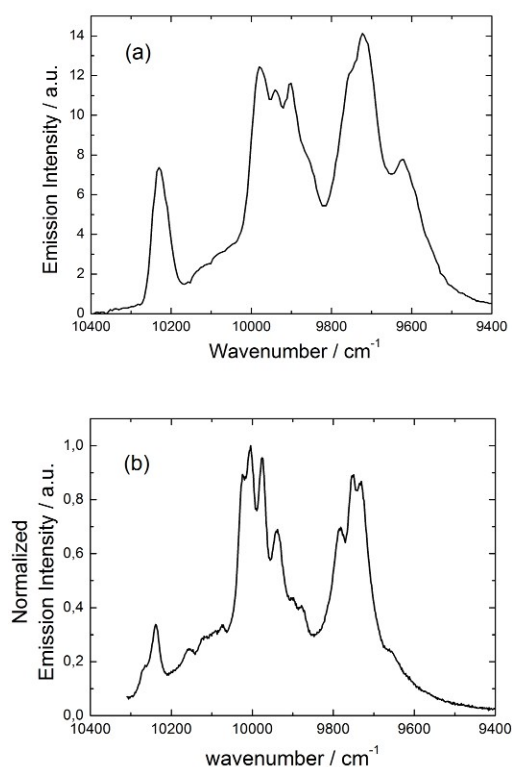
	Energy exp (cm^{-1})	Energy theo (cm^{-1})	Osc.	Type	Assignment	Transition
L	23800	25307	0.04	ILCT	$\pi_{\text{TTF}} \rightarrow \pi^*_{\text{Py-N-oxide}}$	H \rightarrow L (86%)
	29400	30586	0.12	ILCT	$\pi_{\text{TTF}} \rightarrow \pi^*_{\text{Py-N-oxide}}$	H \rightarrow L+5 (22%) H-1 \rightarrow L+1/+2 (15/19%)
	31800	31852	0.07	ID	$\pi_{\text{TTF}} \rightarrow \pi^*_{\text{TTF}}$	H \rightarrow L+5/+6 (44/32%) H \rightarrow L+6 (25%)
	36100	32569	0.24	ILCT	$\pi_{\text{TTF}} \rightarrow \pi^*_{\text{Py-N-oxide}}$	H-1 \rightarrow L (71%)
	40484	32814	0.07			
	40836	40836	0.10	IA	$\pi_{\text{Py-N-oxide}} \rightarrow \pi^*_{\text{Py-N-oxide}}$	H-1 \rightarrow L+6 (43%) + H-
	41000	41455	0.07	ID	$\pi_{\text{TTF}} \rightarrow \pi^*_{\text{TTF}}$	3 \rightarrow L/+2/+3/+4 (14/11/8/9/8%) H \rightarrow L+11 (43%)

Table 7. Absorption data for ligand **L** and coordination complex **3**.

	L (solid-state)	3 (CH ₂ Cl ₂ solution)	3 (solid-state)	Type
Energy exp (cm ⁻¹)	15500	/	15500	Inter-LCT
	18800	22500	19800	ILCT
	23100	28000	22900	ILCT
	/	29900	26900	Itta
	27100	32000	29700	ILCT
	31500	37900	33000	ID
	39200	43900	38500	IL

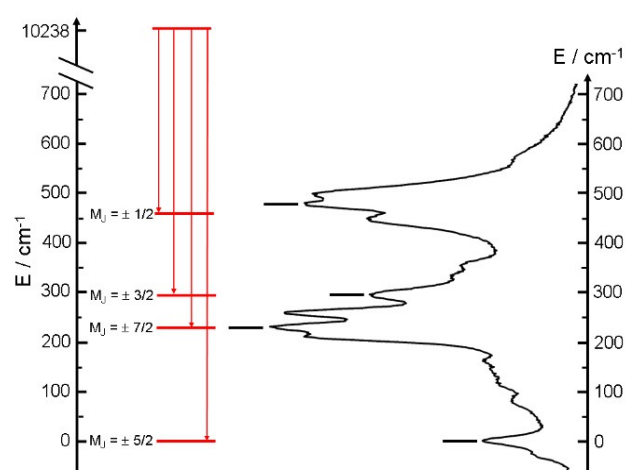
Emission properties.

Emission properties of **3** were measured in solid state at 77 K (Fig. 17a). The characteristic luminescence profile of Yb^{III} corresponding to ²F_{5/2} → ²F_{7/2} transition is observed upon irradiation at 22200 cm⁻¹ (450 nm).

**Fig. 17** Luminescence spectrum of **3** in the NIR range for $\lambda_{\text{ex}} = 22220 \text{ cm}^{-1}$ (450 nm) in solid-state at 77 K (a) and luminescence spectrum obtained by direct irradiation of the f-f transitions (b).

The almost complete absence of any residual ligand-centred emission in the visible region indicates that the energy-transfer process is rather efficient. As already observed in previously published TTF-based complexes of Yb^{III}, the antenna-effect sensitization process is favored and proceeds through energy transfer from the singlet CT state of the **L** chromophore.^{11c-f}

Eight emission maxima and shoulders are clearly identified at the following energies: 9624 cm⁻¹, 9722 cm⁻¹, 9756 cm⁻¹, 9860 cm⁻¹, 9900 cm⁻¹, 9940 cm⁻¹, 9980 cm⁻¹ and 10230 cm⁻¹. This number of contributions is higher than the degeneracy of the ²F_{7/2} ground state (Kramer's doublets) (maximum 4 contributions). By analogy with one of our previous work¹¹ⁱ and the one by Auzel et al.³⁵, the additional emission contributions could be attributed to transitions coming from the second or/and third M_J states of the ²F_{5/2} multiplet state. In order to discriminate between vibronic contribution and contribution of excited multiplet state to explain the origin of these additional bands, emission spectrum was recorded by direct laser excitation of the f-f bands (Fig. 17b).³⁶ The two spectra are very similar although a partial quenching of the lowest-energy contribution (9624 cm⁻¹) by a direct f-f sensitization can be observed and this decrease may be assigned to vibronic contributions. Assuming that the additional emission bands are due to the two M_J excited states of the ²F_{5/2} multiplet, the maximum expected transitions can be twelve. The total splitting is determined equal to 537 cm⁻¹. The values of this splitting for an Yb^{III} ion in a distorted and regular³⁷ D₃ symmetry are 455 cm⁻¹ and 372 cm⁻¹ respectively while a splitting of 528 cm⁻¹ is found for a Yb complex in a lower symmetry up to 880 nm for an organometallic derivative³⁸. The value of 537 cm⁻¹ seems to correspond to a quite low symmetry that is in agreement with the lowest symmetry of the coordination sphere around the Yb^{III} ions in **3** (distorted square anti-prism). In addition, emission spectroscopy provides a direct probe of the ground state multiplet splitting which can be confronted to magnetic data (Fig. 18). Thus the energy splitting of the ²F_{7/2} ground state multiplet extracts from the experimental luminescence (M_J = ± 5/2 (0 cm⁻¹), M_J = ± 7/2 (234 cm⁻¹), M_J = ± 3/2 (300 cm⁻¹) and M_J = ± 1/2 (488 cm⁻¹)) is in perfect agreement with the results of MS-CASPT2/RASSI-SO calculations (M_J = ± 5/2 (0 cm⁻¹), M_J = ± 7/2 (234 cm⁻¹), M_J = ± 3/2 (298 cm⁻¹) and M_J = ± 1/2 (467 cm⁻¹)).

**Fig. 18** The solid state 77 K emission spectra are represented with an appropriate shift of the energy scale. Diagram of energy levels for compounds **3** (full black sticks) given by the main contribution of the luminescence spectra. Labels correspond to the M_J values. Diagram of energy levels for compounds **3** (red sticks) obtained by MS-CASPT2/RASSI-SO calculations.

Conclusions

Three Dy^{III} and Yb^{III} complexes involving the 4,5-ethylenedioxy-4',5'-bis(2-pyridyl-N-oxidemethylthio)tetrathiafulvalene Ligand (**L**) have been reported. The use of hfac⁻ as ancillary ligands for the lanthanide precursor leads to the dinuclear complex **1** while the use of tta⁻ one leads to the mononuclear complexes **2** and **3**. In all the compounds, the lanthanide ion is surrounded by a distorted O8 D_{4d} symmetry environment. The electronic distribution around the Dy^{III} ion in **1** and Yb^{III} ion in **3** favours an Ising system and so to single-molecule magnet behaviours. The Ising character is confirmed by ab initio calculations. Both calculated and experimental anisotropy axis have been determined and are in good agreement. Interestingly compound **2** does not display out-of-phase component of the magnetic susceptibility whereas **1** does even if the nature of the neighbouring atoms and the symmetry of the coordination sphere are the same. That shows that subtle change of the ligands can induce drastic change in the magnetic behaviour. The ligand **L** guarantees an efficient sensitization of the Yb^{III} luminescence by antenna effect and the luminescence data for **3** can be correlated to the magnetic data. **3** thus enlarges the very scarce series of redox-active luminescent SMM.

Acknowledgements

This work was supported by the CNRS, Rennes Métropole, Université de Rennes 1, Région Bretagne, FEDER and Agence Nationale de la Recherche (N° ANR-13-BS07-0022-01).

Notes and references

- (a) A. Dei and D. Gatteschi, *Angew. Chem., Int. Ed.*, 2011, **50**, 11852–11858; (b) M. N. Leuenberger and D. Loss, *Nature*, 2001, **410**, 789–793; (c) S. Hill, R. S. Edwards, N. Aliaga-Alcalde and G. Christou, *Science*, 2003, **302**, 1015–1018; (d) M. Hosseini, S. Rebic, B. M. Sparkes, J. Twamley, B. C. Buchler and P. K. Lam, *Light: Sci. Appl.*, 2012, **1**, e40.
- (a) R. Sessoli, H. L. Tsai, A. R. Schake, S. Wang, J. B. Vincent, K. Folting, D. Gatteschi, G. Christou and D. N. Hendrickson, *J. Am. Chem. Soc.*, 2002, **115**, 1804–1816; (b) M. Mannini, F. Pineider, P. Saintavrit, C. Danieli, E. Otero, C. Sciancalepore, A. M. Talarico, M.-A. Arrio, A. Cornia, D. Gatteschi and R. Sessoli, *Nat. Mater.*, 2009, **8**, 194–197; (c) M. Gu, X. Li and Y. Cao, *Light: Sci. Appl.*, 2014, **3**, e177.
- (a) N. Papisimakis, S. Thongrattanasiri, N. I. Zheludev and F. J. Garcia de Abajo, *Light: Sci. Appl.*, 2013, **2**, e78; (b) S. Sanvito, *Chem. Soc. Rev.*, 2011, **40**, 3336–3355; (c) L. Bogani and W. Wernsdorfer, *Nat. Mater.*, 2008, **7**, 179–186.
- S.-Y. Lin, C. Wang, L. Zhao, J. Wua and J. Tang, *Dalton Trans.*, 2015, **44**, 223.
- J. Long, J. Rouquette, J.-M. Thibaud, R. A. S. Ferreira, L. D. Carlos, B. Donnadieu, V. Vieru, L. F. Chibotaru, L. Konczewicz, J. Haines, Yannick Guari, and Joulia Larionova *Angew. Chem. Int. Ed.* 2015, DOI : 10.1002/anie.201410523.
- X.-L. Li, C.-L. Chen, H.-P. Xiao, A.-L. Wang, C.-M. Liu, X. Zheng, L.-J. Gao, X.-G. Yanga and S.-M. Fang, *Dalton Trans.*, 2013, **42**, 15317–15325.
- (a) J. C. G. Bünzli, and C. Piguet, *Chem. Rev.*, 2002, **102**, 1897; (b) R. Sessoli and A. K. Powell, *Coord. Chem. Rev.*, 2009, **253**, 2328–2341; (c) J. Luzon and R. Sessoli, *Dalton Trans.* 2012, **41**, 13556–13567; (d) T. Tang, I. Hewitt, N. T. Madhu, G. Chastanet, W. Wernsdorfer, C. E. Anson, C. Benelli, R. Sessoli and A. K. Powell, *Angew. Chem. Int. Ed.*, 2006, **45**, 1729–1733.
- (a) J.-C. G. Bünzli, *Acc. Chem. Res.* 2006, **39**, 53–61; (b) S. V. Eliseeva and J.-C. G. Bünzli, *Chem. Soc. Rev.*, 2010, **39**, 189–227; (c) S. V. Eliseeva, J.-C. G. Bünzli in Chap 1 Springer series on fluorescence, Vol. 7, Lanthanide spectroscopy, Materials, and Bio-applications, ed.P; Hännen and H. Härmä, Springer Verlag, Berlin, Vol. 7, 2010. (d) Luminescence of Lanthanide Ions in Coordination Compounds and Nanomaterials Ed. By A. De Bettencourt-Diaz, Wiley 2014.
- (a) H. Tanaka, H. Kobayashi, A. Kobayashi and P. Cassoux, *Adv. Mater.*, 2000, **12**, 1685–1689; (b) S. Uji, H. Shinagawa, T. Terashima, C. Terakura, T. Yakabe, Y. Terai, M. Tokumoto, A. Kobayashi, H. Tanaka and H. Kobayashi, *Nature*, 2001, **410**, 908–910; (c) A. Kobayashi, E. Fujiwara and H. Kobayashi, *Chem. Rev.* 2004, **104**, 5243–5264; (d) T. Enoki and A. Miyasaki, *Chem. Rev.*, 2004, **104**, 5449–5478; (e) E. Coronado and P. Day, *Chem. Rev.*, 2004, **104**, 5419–5448; (f) L. Ouahab and T. Enoki, *Eur. J. Inorg. Chem.* 2004, 933–941; (g) H. Fujiwara, K. Wada, T. Hiraoka, T. Hayashi, T. Sugimoto, H. Nakazumi, K. Yokogawa, M. Teramura, S. Yasuzuka, K. Murata and T. Mori, *J. Am. Chem. Soc.* 2005, **127**, 14166–14167; (h) R. Kato, *Bull. Chem. Soc. Jpn.*, 2000, **73**, 515–534; (i) D. Lorcy, N. Bellec, M. Fourmigué and N. Avarvari, *Coord. Chem. Rev.*, 2009, **253**, 1398–1438 and references therein; (j) F. Pointillart, S. Golhen, O. Cador, L. Ouahab, *Dalton Trans.*, 2013, **42**, 1949–1960 and references therein.
- (a) S. Faulkner, B. P. Burton-Pye, T. Khan, L. R. Martin, S. D. Wray and P. J. Skabara, *Chem. Commun.*, 2002, **16**, 1668–1669; (b) S. J. A. Pope, B. P. Burton-Pye, R. Berridge, T. Khan, P. Skabara and S. Faulkner, *Dalton Trans.*, 2006, 2907–2912; (c) F. Pointillart, T. Cauchy, O. Maury, Y. Le Gal, S. Golhen, O. Cador and L. Ouahab, *Chem.-Eur. J.*, 2010, **16**, 11926–11941; (d) F. Pointillart, A. Bourdolle, T. Cauchy, O. Maury, Y. Le Gal, S. Golhen, O. Cador, and L. Ouahab, *Inorg. Chem.*, 2012, **51**, 978–984; (e) A. D'Aléo, F. Pointillart, L. Ouahab, C. Andraud, O. Maury, *Coord. Chem. Rev.* 2012, **256**, 1604–1620; (f) F. Pointillart, B. Le Guennic, S. Golhen, O. Cador, O. Maury and L. Ouahab, *Inorg. Chem.* 2013, **52**, 1610–1620; (g) M. Feng, F. Pointillart, B. Le Guennic, B. Lefeuvre, S. Golhen, O. Cador, O. Maury and L. Ouahab, *Chem. Asian. J.* 2014, **9**, 2814–2825. (h) F. Pointillart, B. Le Guennic, T. Cauchy, S. Golhen, O. Cador, O. Maury and L. Ouahab, *Inorg. Chem.*, 2013, **52**, 5978–5990.
- (a) G. Cucinotta, M. Perfetti, J. Luzon, M. Etienne, P. E. Car, A. Caneschi, G. Calvez, K. Bernot and R. Sessoli, *Angew. Chem. Int. Ed.* 2012, **51**, 1606–1610; (b) M.-E. Boulon, G. Cucinotta, J. Luzon, C. Degl'Innocenti, M. Perfetti, K. Bernot, G. Calvez, A. Caneschi and R. Sessoli, *Angew. Chem. Int. Ed.*, 2013, **52**, 350–354; (c) F. Pointillart, B. Le Guennic, S. Golhen, O. Cador, O. Maury, L. Ouahab, *Chem. Commun.*, 2013, **49**, 615–617; (d) J. Long, R. Vallat, R. A. S. Ferreira, L. D. Carlos, F. A. A. Paz, Y. Guari and J. Larionova, *Chem. Commun.*, 2012, **48**, 9974–9976; (e) K. Yamashita, R. Miyazaki, Y. Kataoka, T. Nakanishi, Y. Hasegawa, M. Nakano, T. Yamamura and T. Kajiwara, *Dalton Trans.*, 2013, **42**, 1987–1990; (f) K. Ehama, Y. Ohmichi, S. Sakamoto, T. Fujinami, N. Matsumoto, N. Mochida, T. Ishida, Y. Sunatsuki, M. Tsuchimoto and N. Re, *Inorg. Chem.* 2013, **52**, 12828–12841; (g) M. Ren, S.-S. Bao, R. A. S. Ferreira, L.-M. Zheng and L. D. Carlos, *Chem. Commun.*, 2014, **50**, 7621–7624; (h) G. Cosquer, F. Pointillart, J. Jung, B. Le Guennic, S. Golhen, O. Cador, Y. Guyot, A. Brenier, O. Maury and L. Ouahab, *Eur. J. Inorg. Chem.* 2014, 69–82; (i) X. Yi, K. Bernot, V. Le Corre, G. Calvez, F. Pointillart, O. Cador, B. Le Guennic, J. Jung, O. Maury, V. Placide, Y. Guyot, T. Roisnel, C.

- Daiguebonne and O. Guillou, *Chem. Eur. J.*, 2014, **20**, 1569-1576.
- 12 (a) J. J. Baldovi, J. M. Clemente-Juan, E. Coronado, Y. Duan, A. Gaita-Arino and C. Gimenez-Saiz, *Inorg. Chem.* 2014, **53**, 9976-9980; (b) J. J. Baldovi, J. M. Clemente-Juan, E. Coronado and A. Gaita-Arino, *Inorg. Chem.*, 2014, **53**, 11323-11327; (c) N. F. Chilton, D. Collison, E. J. L. McInnes, R. E. P. Winpenny and A. Soncini, *Nat. Commun.*, 2013, **4**, 2551-2558; (d) C. Y. Chow, H. Bolvin, V. E. Campbell, R. Guillot, J. F. Kampf, W. Werndorfer, F. V. Gendron, J. Autschbach, V. L. Pecoraro, T. Mallah, *Chem. Sci.* **2015**, DOI: 10.1039/C5SC01029B; (e) L. Ungur, S.-Y. Lin, J. Tang, L. F. Chibotaru, *Chem. Soc. Rev.*, 2014, **43**, 6894-6905; (f) Y.-N. Guo, G.-F. Xu, W. Werndorfer, L. Ungur, Y. Guo, J. Tang, H.-J. Zhang, L. F. Chibotaru, A. K. Powell, *J. Am. Chem. Soc.*, 2011, **133**, 11948-11951.
- 13 M. F. Richardson, W. F. Wagner, D. E. Sands, *J. Inorg. Nucl. Chem.*, 1968, **30**, 1275-1289.
- 14 A. I. Vooshin, N. M. Shavaleev, V. P. Kazakov, *J. Luminescence*, 2000, **91**, 49-58.
- 15 (a) N. Sevenstrup, K. M. Rasmussen, T. K. Hansen and J. Becher, *Synthesis*, 1994, **8**, 809; (b) M. Xu, Y. Ji, J. L. Zuo and X. Z. You, *J. Heterocycl. Chem.*, 2005, **42**, 847; (c) L. Binet, J. M. Fabre, C. Montginoul, K. B. Simonsen and J. Becher, *J. Chem. Soc., Perkin Trans. 1*, 1996, **8**, 783.
- 16 M. Polasek, M. Sedinova, J. Kotek, L. V. Elst, R. N. Muller, P. Hermann and I. Lukes, *Inorg. Chem.*, 2009, **48**, 455.
- 17 SHELX97 - Programs for Crystal Structure Analysis (Release 97-2). Sheldrick, G. M. Institut für Anorganische Chemie der Universität, Tammanstrasse 4, D-3400 Göttingen, Germany, 1998. SIR97 - A. Altomare, M. C. Burla, M. Camalli, G. L. Casciarano, C. Giacovazzo, A. Guagliardi, A. G. Moliterni, G. Polidori and R. Spagna, *J. Appl. Cryst.*, 1999, **32**, 115-119.
- 18 M. J. Frisch, G. W. Trucks, H. B. Schlegel, G. E. Scuseria, M. A. Robb, J. R. Cheeseman, G. Scalmani, V. Barone, B. Mennucci, G. A. Petersson, H. Nakatsuji, M. Caricato, X. Li, H. P. Hratchian, A. F. Izmaylov, J. Bloino, G. Zheng, J. L. Sonnenberg, M. Hada, M. Ehara, K. Toyota, R. Fukuda, J. Hasegawa, M. Ishida, T. Nakajima, Y. Honda, O. Kitao, H. Nakai, T. Vreven, Jr. J. A. Montgomery, J. E. Peralta, F. Ogliaro, M. Bearpark, J. J. Heyd, E. Brothers, K. N. Kudin, V. N. Staroverov, R. Kobayashi, J. Normand, K. Raghavachari, A. Rendell, J. C. Burant, S. S. Iyengar, J. Tomasi, M. Cossi, N. Rega, J. M. Millam, M. Klene, J. E. Knox, J. B. Cross, V. Bakken, C. Adamo, J. Jaramillo, R. Gomperts, R. E. Stratmann, O. Yazyev, A. J. Austin, R. Cammi, C. Pomelli, J. W. Ochterski, R. L. Martin, K. Morokuma, V. G. Zakrzewski, G. A. Voth, P. Salvador, J. J. Dannenberg, S. Dapprich, A. D. Daniels, O. Farkas, J. B. Foresman, J. V. Ortiz, J. Cioslowski and D. J. Fox, Gaussian 09 Revision A.02, Gaussian Inc., Wallingford CT, **2009**.
- 19 (a) J. P. Perdew, K. Burke and M. Ernzerhof, *Phys. Rev. Lett.*, 1996, **77**, 3865-3868; (b) C. Adamo and V. Barone, *J. Chem. Phys.*, 1999, **110**, 6158-6170.
- 20 F. Weigend and R. Ahlrichs, *Phys. Chem. Chem. Phys.*, 2005, **7**, 3297-3305.
- 21 J. Tomasi, B. Mennucci and R. Cammi, *Chem. Rev.*, 2005, **105**, 2999-3093.
- 22 (a) M. Cossi and V. Barone, *J. Chem. Phys.*, 2001, **115**, 4708-4717; (b) R. Improta, V. Barone, G. Scalmani and M. J. Frisch, *J. Chem. Phys.*, 2006, **125**, 054103-054109.
- 23 A.-R. Allouche, *J. Comput. Chem.*, 2011, **32**, 174-182.
- 24 F. Aquilante, L. De Vico, N. Ferré, G. Ghigo, P.A. Malmqvist, P. Neogady, T. Bondo Pedersen, M. Pitonak, M. Reiher, B. O. Roos, L. Serrano-Andrés, M. Urban, V. Veryazov and R. Lindh, *J. Comput. Chem.*, 2010, **31**, 224-247.
- 25 B. O. Roos, P. R. Taylor and P. E. M. Siegbahn, *Chem. Phys.*, 1980, **48**, 157-288.
- 26 (a) P. A. Malmqvist, B. O. Roos, B. Schimmelpfennig, *Chem. Phys. Lett.*, 2002, **357**, 230-240; (b) P. A. Malmqvist, B. O. Roos, *Chem. Phys. Lett.*, 1989, **155**, 189-194.
- 27 (a) L. F. Chibotaru and L. Ungur, *J. Chem. Phys.*, 2012, **137**, 064112-064122; (b) L. F. Chibotaru, L. Ungur and A. Soncini, *Angew. Chem., Int. Ed.*, 2008, **47**, 4126-4129.
- 28 F. Aquilante, P.-A. Malmqvist, T.-B. Pedersen, A. Ghosh and B. O. Roos, *J. Chem. Theory Comput.*, 2008, **4**, 694-702.
- 29 (a) B. O. Roos, R. Lindh, P.-A. Malmqvist, V. Veryazov and P.-O. Widmark, *J. Phys. Chem. A*, 2004, **108**, 2851-2858; (b) B. O. Roos, R. Lindh, P.-A.; Malmqvist, V. Veryazov and P.-O. Widmark, *J. Phys. Chem. A*, 2005, **109**, 6576-6586; (c) B. O. Roos, R. Lindh, P.-A. Malmqvist, V. Veryazov, P.-O. Widmark and A. C. Borin, *J. Phys. Chem. A*, 2008, **112**, 11431-11435.
- 30 M. Llunell, D. Casanova, J. Cirera, J. M. Bofill, P. Alemany and S. Alvarez, S. SHAPE (version 2.1), Barcelona, 2013.
- 31 F. Habib, P.-H. Lin, J. Long, I. Korobkov, W. Werndorfer and M. Murugesu, *J. Am. Chem. Soc.*, 2011, **133**, 8830.
- 32 G. Cosquer, F. Pointillart, S. Golhen, O. Cador and L. Ouahab, *Chem. Eur. J.*, 2013, **19**, 7895-7903.
- 33 (a) J. Jung, T. da Cunha, B. Le Guennic, F. Pointillart, L. M. Pereira, J. Luzon, S. Golhen, O. Cador, O. Maury and L. Ouahab, *Eur. J. Inorg. Chem.*, 2014, 3888-3894; (b) F. Pointillart, J. Jung, R. Berraud-Pache, B. Le Guennic, V. Dorcet, S. Golhen, O. Cador, O. Maury, Y. Guyot, S. Decurtins, S.-X. Liu and L. Ouahab, *Inorg. Chem.*, 2015, **54**, 5384-5397.
- 34 G. Cosquer, F. Pointillart, B. Le Guennic, Y. Le Gal, S. Golhen, O. Cador and L. Ouahab, *Inorg. Chem.*, 2012, **51**, 8488-8501.
- 35 P. Goldner, F. Pell, D. Meichenin and F. Auzel, *J. Lumin.*, 1997, **71**, 137-150.
- 36 G. Zucchi, R. Scopelliti, P.-A. Pittet, J.C. G. Bünzli and R. D. Rogers, *J. Chem. Soc., Dalton Trans.*, 1999, 931-938.
- 37 F. R. Gonçalves Silva, O. L. Malta, C. Reinhard, H. U. Güdel, C. Piguet, J. Moser and J.-C. G. Bünzli, *J. Phys. Chem. A*, 2002, **106**, 1670-1677.
- 38 G. Lapadula, A. Bourdolle, F. Allouche, M. Conley, I. del Rosa, L. Maron, W. W. Lukens, Y. Guyot, C. Andraud, S. Bresselet, C. Copéret, O. Maury and R. A. Andersen, *Chem. Mater.*, 2014, **26**, 1062-1073.